第 34 卷第 9 期
2018 年 9 月

无 机 化 学 学 报
CHINESE JOURNAL OF INORGANIC CHEMISTRY

Vol.34 No.9
1710-1718

钛掺杂钙钛矿制备高效率钙钛矿太阳能电池

田 辉 熊 启 刘 鹏 张 京* 韩 磊 张宇豪 郑永进 吴立爽 诸跃进*
(宁波大学理学院,微电子科学与工程系,宁波 315211)

摘要:采用钛离子掺杂钙钛矿薄膜的方法修饰钙钛矿晶界缺陷。研究表明钛离子富集在晶界处,有效地钝化了晶界缺陷,同时有助于连续、平整、高质量薄膜的形成。经过钛离子掺杂后的钙钛矿太阳能电池电流(J_{SC})达到 22.3 mA·cm^{-2},开路电压(V_{OC})达 1.1 V,填充因子(FF)高达 72.4%,光电转换效率(PCE)优化至 17.4%,远高于未掺杂钙钛矿太阳能电池。

关键词:钙钛矿太阳能电池;钛掺杂;缺陷态;晶界
中图分类号:O469 **文献标识码**:A **文章编号**:1001-4861(2018)09-1710-09
DOI:10.11862/CJIC.2018.200

Ti^{4+} Doped Perovskite for Efficient Perovskite Solar Cells by Grain Boundary Passivation

TIAN Hui XIONG Qi LIU Peng ZHANG Jing* HAN Lei
ZHANG Yu-Hao ZHENG Yong-Jin WU Li-Shuang ZHU Yue-Jin*
(*Department of Microelectronic Science and Engineering, Faculty of Science, Ningbo University, Ningbo, Zhejiang* 315211, *China*)

Abstract: The grain boundaries defect is solved by titanium ion (Ti^{4+}) doping. Ti^{4+} has small radius which is proved to form at the grain boundary of polycrystalline perovskite. By control doping of titanium ion, grain size become more uniform, which leads to more continuous perovskite thin film. Studies suggest that the defects in grain boundary of polycrystalline perovskite are passivated by doping Ti^{4+}, which results in the trap states concentration greatly decrease. And experimental test clearly exhibits more excellent performance of short-circuit current density (J_{SC}=22.3 mA·cm^{-2}), open-circuit voltage (V_{OC}=1.10 V), fill factor (FF=72.4%) and photovoltaic conversion efficiency (PCE=17.4%) with low amount Ti^{4+} doping compared with pure planar heterojunction perovskite solar cells (AM1.5).

Keywords: perovskite solar cells; Ti^{4+} doping; defect states; grain boundary

In the past several years, organic-inorganic perovskite solar cells have become one of the most studied cells for their high efficiency, low fabrication cost and easy solution process[1-5]. The core component is the perovskite layer in n-i-p type perovskite solar cells (PSCs), whose properties are quite important for efficient charge transport. As the light absorption layer, perovskite layer generates electron/hole carriers, which are separated and driven to corresponding n and p sides under the effect of built-in internal electrical field. Then, they pass through electron/hole transport layer (ETL/HTL) to converging in electrode[6-7]. There are two types of defects in perovskite layer: (1) Deep level intrinsic defects which result in the recombination and trap states in perovskite lattice[8-9]; (2) Owing to polycrystalline structure of perovskite, a large amount of defects appear in the poly crystal perovskite grain boundary during solution-based prep-

收稿日期:2018-03-31。收修改稿日期:2018-06-11。
国家自然科学基金(No.11374168,11547033)、省自然科学基金(No.LY18F040004)、国家留学归国人员基金和宁波大学王宽诚基金项目资助。
*通信联系人。E-mail:zhangjing@nbu.edu.cn; zhuyuejin@nbu.edu.cn

aration processes[8]. The large number of trap states nevertheless induce charge carrier recombination and limit the PCE in thin-film solar cells unless they can be further reduced[10]. Moreover, the trap states cast awful impact on hysteresis properties, leading to stability concerns over the devices[11]. Thus, lowering the charge recombination via reducing defects states in the perovskite polycrystalline thin film is crucial for continued progress in device performance.

Up to now, three reported methods are certified to solve defect problem produced in the perovskite layer. Firstly, adding functional molecules to act on the grain boundary can effectively passivate the trap states. Insulating polymers, ionic liquid and the semiconducting molecule fullerene are reported to form chemical interactions with the surface atoms thus passivate the trap states[12-13]. Secondly, adding an interface layer above perovskite layer effectively illuminates the surface trap states and reduce the interface recombination[14-15]. Thirdly, the extrinsic metal ions (alkali metal ions K^+, Na^+, Zn^{2+}) are added in the perovskite films to effectively influence the crystallinity and passivate the trap states[16-18].

In this work, we report a method to improve properties with Ti^{4+} doping in perovskite precursor solution to passivate defect in perovskite. Once investigating the effect of Ti^{4+}, it is found that most of Ti^{4+} was distributed in the polycrystalline perovskite grain boundary. Further research shows size of perovskite grain changed subtly. The bandgap of doped perovskite unchanged after Ti^{4+} doping. And the photoluminescence and carrier transport are obviously enhanced, indicating the trap states are effectively reduced. With optimum content of Ti^{4+} concentration doped in perovskite precursor solution, the efficiency (17.4%) of PSCs demonstrated significant improvement contrast with conventional device (14.0%). Higher efficiency suggests it is an effective method via doping engineering with Ti^{4+}.

1　Experimental

1.1　Fabrication of perovskite solar cell device

The original PSCs are composed of FTO layer/TiO_2 blocking layer/$CH_3NH_3PbI_3$ ($MAPbI_3$) layer/spiro-OMeTAD/Ag. The pure perovskite precursor solution was prepared by directly mixing $CH_3NH_3I_3$ and PbI_2 with $n_{CH_3NH_3I_3}$:n_{PbI_2}=1:1 in dimethylformamide (DMF). The pure $CH_3NH_3PbI_3$ is a conventional contrast sample. $TiCl_4$ ethyl alcohol solution (1 mol·L^{-1}) is added to perovskite precursor solution. Different volume of $TiCl_4$ solution is add to make a series of doped perovskite precursor solution with different molar ratios (x%, x=0, 0.05, 0.1, 0.2 and 0.5) of Ti to Pb. Ti^{4+}-x% represents with different concentrations of Ti^{4+} doped the samples. The 60 nm thick TiO_2 compact layer was synthesized in air via sol-gel method and deposited on the etched and cleaned FTO glass. Titanium (Ⅳ) isopropoxide was added to the mixed solution of isopropanol alcohol, diethanolamine and deionized water then the sol was left stirring for 1 h before using. The deposited TiO_2 film was annealed in oven for 30 min at 450 ℃[19]. Next, the compact TiO_2 layer was treated with 0.04 mol·L^{-1} $TiCl_4$ at 70 ℃ for 30 min and sintered in oven for 30 min at 500 ℃.

Perovskite layer was deposited on the TiO_2 blocking layer by spinning coating the perovskite precursor solution at 2 800 r·min^{-1} for 30 s and treated by anti-solvent chlorobenzene (CB). Then, the substrate was carefully baked on the hot plate to form uniform perovskite film by slow annealing. The hole transport layer was prepared by spinning coating hole transport material (HTM) solution at 3 000 r·min^{-1} for 30 s. HTM solution consists of 60 mmol·L^{-1} 2,2′,7,7′-tetrakis (*N*,*N*-di-*p*-methox-yphenylamine)-9,9′-spirobifluorene (spiro-MeOTAD) in chlorobenzene with added 80%(*n*/*n*) 4-tert-butylpyridine (tBP) and 30%(*n*/*n*) of lithium bis(trifluoromethanesulfony)imide (Li-TFSI)[20]. Then, substrate would be oxidized in dry air for 6 h. Lastly, approximately 100 nm of Ag electrode were evaporated on the HTM with ultrahigh vacuum.

1.2　Characterization of the devices

X-ray diffraction patterns (XRD) of the Ti^{4+} doped perovskite films based on FTO glass were acquired by a Bruker instrument (D8 advance, made in Germany) using Cu radiation (λ=0.154 06 nm, applied voltage of 40 kV and current of 800 mA) at scan rate of 4°·min^{-1}

and range of 10°~50° for crystal structure and size. The surface morphologies and element analysis of the perovskite films (FTO glass/perovskite layer) were observed by a scanning electron microscope (SEM, Hitachi, SU-70, Japan) with energy dispersive X-ray spectroscopy (EDX). The optical absorption spectrum of the perovskite films based on glass was tested by UV-TR spectrophotometer (Agilent Cary 5000, USA). Steady-state photoluminescence (PL) of the perovskite films was measured by fluorescence spectrophotometer (Agilent, USA) with 532 nm light to excite the two groups of substrates that were respectively based on glass/perovskite and FTO glass/perovskite. Time-resolved PL spectra (excited at 450 nm; monitored at 750 nm) were recorded on Horiba fluorescence spectrometer. The binding energies of the perovskite elements were analyzed by X-ray photoelectron spectroscopy (XPS, Shimadzu, Japan) using Al $K\alpha$ radiation. Current-voltage (J-V) characteristics were measured by the equipment consisting of a Keithley 4200 semiconductor analyzer and a sunlight simulator (Newport solar simulator 3A, AM1.5, 100 mW·cm^{-2}) requiring to be adjusted with a piece of standard silicon reference cell. The electrochemical impedance spectroscopy (EIS) of perovskite solar cells were measured with an electrochemical workstation (Zennium, Germany).

2 Results and discussion

2.1 Crystalline and surface morphology of $CH_3NH_3PbI_3$

The crystallinity and continuity of the perovskite film are key factors for charge dissociation and charge transmission in device. The XRD patterns of perovskite film with different concentration of Ti^{4+} on FTO glass is shown in Fig.1a, which indicates the change of crystallinity and half-peak width. In Fig.1a, the peaks at 14.06°, 28.40° and 43.30° are respectively assigned to the (110), (220) and (330) planes of $CH_3NH_3PbI_3$[21]. The doped Ti^{4+} has ionic radius of 0.064 nm, far smaller than the Pb^{2+} of 0.119 nm. Moreover, Ti has 4 valence electrons to coordinate while Pb has 2 valence electrons to coordinate in $CH_3NH_3PbI_3$. Therefore, great discrepancy of ionic size and valence states indicates that Ti^{4+} is hardly to substitute the Pb^{2+} in $CH_3NH_3PbI_3$. The XRD patterns show the perovskite peak position almost does not shift with doping concentration increasing, which illuminates Ti^{4+} does not change the crystalline lattice and therefore Ti^{4+} is not substitutional impurity in the perovskite crystalline. Furthermore, it is noticed that the peak intensity is higher with Ti^{4+}-0.05% and Ti^{4+}-0.1% doped perovskite, compared with the pure one. It means that the crystallinity of doped perovskite is better than that of the pure perovskite. Gradually increasing the Ti^{4+} amount, the XRD peak intensity decreased further, which means the crystallinity of perovskite based on Ti^{4+} with 0.2%~0.5% is worse than of the pure perovskite film. The average size of perovskite grain is circulated according to half-peak width of the perovskite (110) diffraction peaks site based on the Scherrer equation as following:

$$D=k\lambda/(\beta\cos\theta)$$

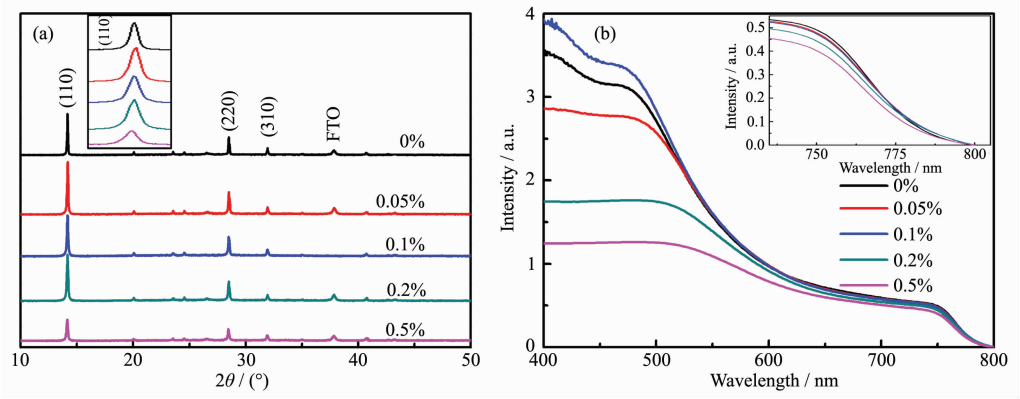

Fig.1 (a) XRD patterns of Ti^{4+} doped perovskite film, the inset is the enlarged (110) diffraction peaks; (b) UV-Vis absorption spectra of perovskite films on glass with and without Ti^{4+}, the insert is the enlarged spectra of (b)

Table 1　Peak position, half-peak width and the calculated grain size of (110) plane

Sample	Peak position / (°)	Half-peak width / (°)	Grain size / nm
Ti^{4+}-0%	14.174	0.091	87.3
Ti^{4+}-0.05%	14.184	0.119	66.3
Ti^{4+}-0.1%	14.164	0.130	60.9
Ti^{4+}-0.2%	14.174	0.130	60.5
Ti^{4+}-0.5%	14.163	0.148	53.3

where D is the crystalline size, λ is the wavelength of X-ray radiation (0.154 nm), k is the constant taken as 0.89, β is the half-peak width, θ is the peak site of the perovskite (110) diffraction peaks in XRD patterns. As shown In Table 1, the size of perovskite grain gradually decreases with the concentration of Ti^{4+} increasing, which reveals Ti^{4+} as dopant diminishes the size of perovskite grain.

The optic band gap change was detected. In UV-IR spectra of the perovskite films upon cleaned glass (Fig.1b), the absorption of Ti^{4+}-0.1% doped perovskite is the highest of the films, which is ascribed to the high quality and the compactness of the film. The absorption onset and the band edge near 800 nm are enlarged to check the bandgap of the perovskite. It is obvious that the absorption onset has no obvious change with Ti^{4+} doping, which reveals that Ti^{4+} ions have no effect on bandgap, and further verifies Ti^{4+} does not substitute Pb^{2+} to form perovskite structure to modify the energy band gap.

2.2　Exploration distribution of Ti^{4+} in perovskite

The top view morphologies of perovskite films were observed by SEM. As is shown in Fig.2(a~c), the size of perovskite grain becomes smaller and more uniform with Ti^{4+}-0.1% and Ti^{4+}-0.2% modification (Fig.2(b,c)) than of the pure perovskite grain in Fig.2a, which may be helpful to form continuous film and produce better contact between perovskite layer and HTL[22].

The element distribution of perovskite films is further researched. In Fig.2d, polycrystal perovskite film structure and the pinholes between the grain boundaries can be observed under SEM-EDS mapping mode. The SEM-mapping of Ti^{4+}-0.1% perovskite film shows the distribute condition of Pb and Ti in polycrystalline perovskite film (Fig.2(e,f)). *In-situ* mapping of lead indicates that Pb is uniformly distributed inside the perovskite films (Fig.2e). By

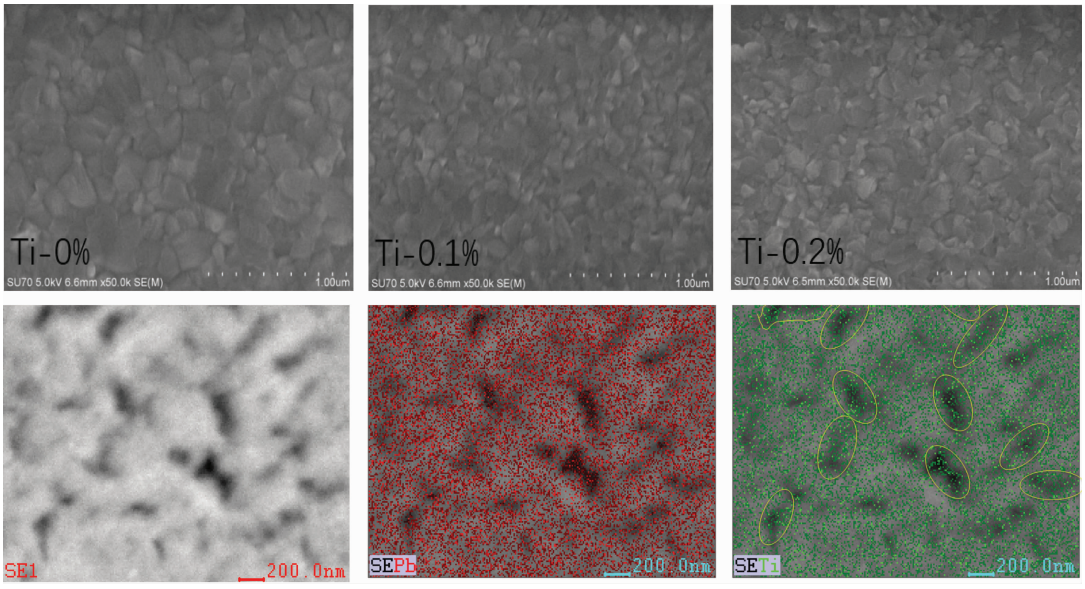

Fig.2　SEM images of Ti^{4+} with (a) 0, (b) 0.1% and (c) 0.2% perovskite film; (d) Surface morphology exposed under SEM-EDS; SEM-mapping of (e) Pb^{2+} and (f) Ti^{4+}

contrast, Ti is intensively distributed at the grain boundaries of polycrystalline perovskite as indicates by the yellow circles in Fig.2f. The above results demonstrate that Ti^{4+} ions are mostly distributed at grain boundary of polycrystalline perovskite as additive. By this way, controlling proper Ti^{4+} dopant might lead to the defect of grain boundary passivated, which alleviates the tendency of non-radiative recombination to carriers by trap states in the grain boundary of polycrystalline perovskite. Meanwhile, controlling proper Ti^{4+} dopant not only diminishes the size of polycrystalline perovskite grain to homogenize the scale of perovskite grain, it also promotes high quality crystallinity of perovskite to be favorable for charge transport.

When Ti^{4+} is formed at the grain boundary of perovskite films, it does not change the perovskite crystalline lattice structure for not substituting the Pb position. However, Ti^{4+} will interact with the atoms in the perovskite material. Fig.3(a,b) indicates the XPS core level spectra of Pb4*f* and I3*d*, respectively. It is clear that the peak positions of Pb4*f* and I3*d* moves to lower binding energy when Ti-0.1% is doped in. Because the Ti will also interact with I, the binding energy of Pb is reduced. On the other hand, Cl is introduced in the system which might also interact with Pb, thus the binding energy of I is also reduced. The scheme of the Ti doping position is indicated in Fig.3c, which also indicates the interaction of Ti with the atoms in $MAPbI_3$.

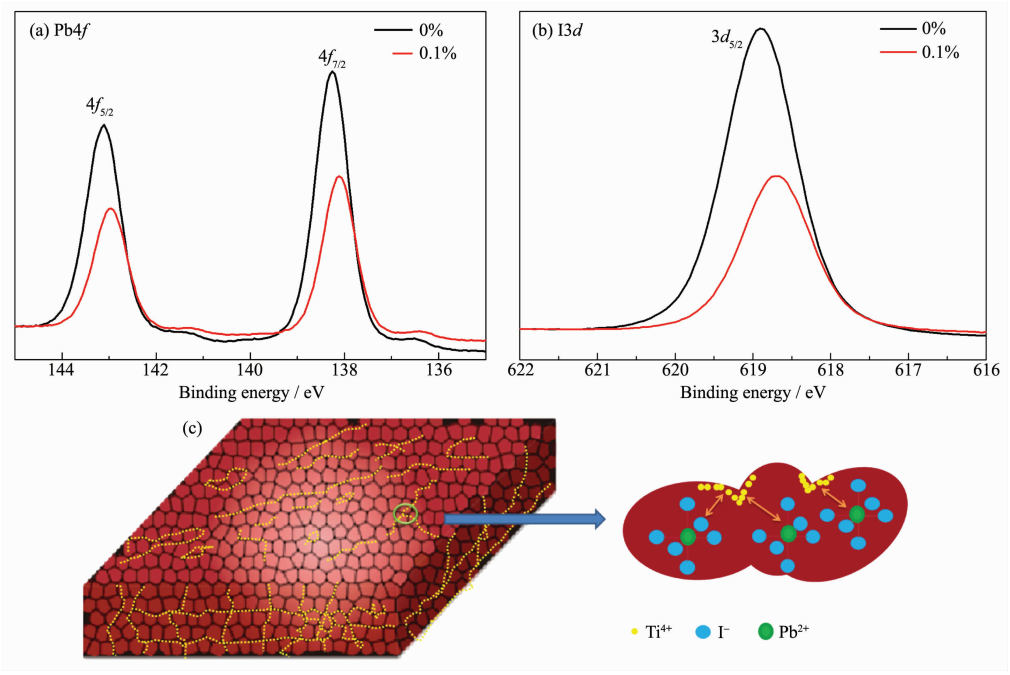

Fig.3 XPS core level spectra of (a) Pb4*f*; and (b) I3*d*; (c) Schema of Ti^{4+} formed at the grain boundary (left), the enlarged grains and the Ti^{4+} interaction with I^- in the film

2.3 Charge transport properties of $CH_3NH_3PbI_3$

To investigate the trap states and charge transport properties in Ti^{4+} doped perovskite materials, the PL spectra of perovskite film on glass and on FTO are investigated. Fig.4a is the steady state PL spectra of perovskite films on glass substrates. Obviously, the peak site of emission light does not change which accounts for Ti^{4+} doping did not influence the bandgap. Furthermore, it is found that the peak intensity of Ti^{4+}-0.05%, Ti^{4+}-0.1% doped perovskite significantly rises compared to the conventional sample. The phenomenon suggests few Ti^{4+}-doped perovskite film effectively restrains the recombination from carriers and trap states, which is benefit for the charge transport. It is demonstrated that grain boundary modification weakens non-radiative recombination[23], which influences luminescence yields and power conversion efficiency[24-26]. Knowing that Ti^{4+} ions does not directly affect lattice,

it just affects the grain size and grain boundary, therefore, it is the Ti^{4+} passivates the trap states at the perovskite grain boundary. However, the PL peak intensity gradually declines with further increasing the dopant density which is due to the decreased crystalline property indicated by XRD in Fig.1a. Fig. 4b is the PL of perovskite films deposited on FTO substrates. Clearly, peak intensity decreased with enhancing the dopant content, which powerfully explains traces of Ti^{4+} ions intensify the ability of carrier extraction from the perovskite to the FTO. By analyzing the PL spectra, it is found that the best concentration is Ti^{4+}-0.1%, with the lowest recombination and highest charge transport property. Therefore, when Ti^{4+}-0.1% ions are doped in perovskite film, it effectively reduces trap states density, block non-radiative recombination and lead to effective charge transport between perovskite layer and ETL/HTL.

To further investigate the charge transport process with and without Ti^{4+} doped perovskite film, the time-resolved PL (TR-PL) measurements of perovskite films on TiO_2 substrate were carried out. The PL decay curves obey a bi-exponential decay function with a fast decay process and a slow decay process through curves fitting in Fig.4c. In general, the fast decay process derives from photo-excited carriers trapped by the defect or sharply transporting to electron/hole interlayer, however, the slow decay process displays the irradiative decay process[27-28]. And the related parameters of TR-PL decay of the sample with and without Ti^{4+} are shown in Table 2. Clearly, the Ti-0.1% doped perovskite curve is higher than the undoped one during the fast decay process, which means reduction of non-radiative recombination process; nevertheless, the Ti-0.1% doped perovskite curve decays more rapidly than original curve during

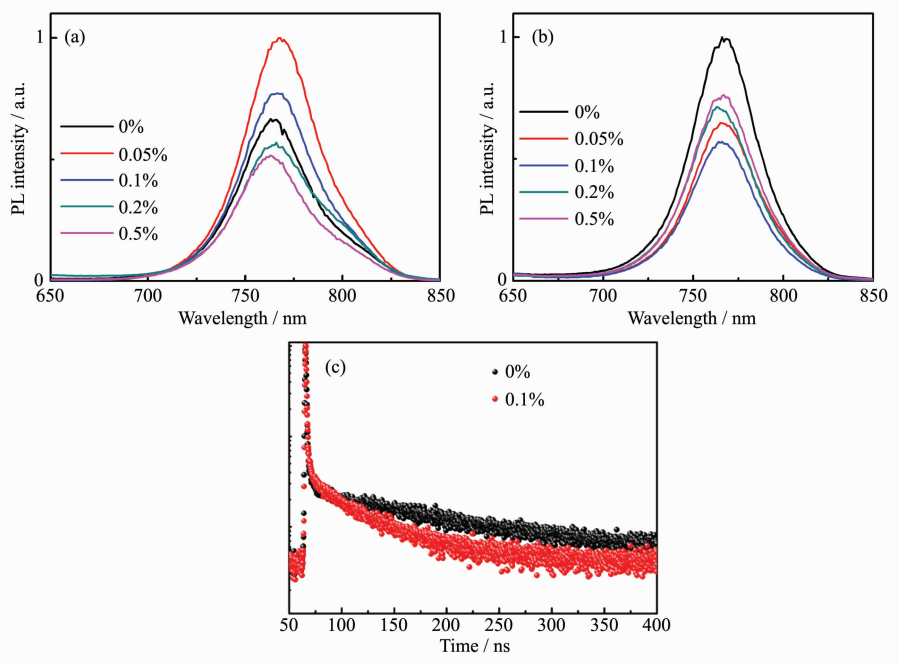

Fig.4　Steady state PL spectra of perovskite film on glass (a) and on FTO (b); (c) Time-resolved PL (TR-PL) spectra of perovskite film on TiO_2 layer

Table 2　Fitting parameters of TR-PL decay curves to perovskite on TiO_2 layer

Sample	A_1	t_1 / ns	A_2	t_2 / ns	t_{avs} / ns
Ti^{4+}-0%	49.1%	3.77	50.9%	144.71	75.49
Ti^{4+}-0.1%	35.7%	5.89	64.3%	56.46	38.43

Notes: t_1 and t_2 present the lifetimes of fast decay and slow decay, respectively; A_1 and A_2 are the proportions of fitting curves representing the fast decay and slow decay parts, respectively; t_{avs} is the lifetime of carriers.

the slow decay process, which means stronger ability of extraction carrier. The phenomenon explains passivated perovskite has less defect states and better charge extraction to the electrode[29]. The average lifetime is 75.49 ns for pure sample, while the average lifetime is 38.43 ns for Ti^{4+}-0.1% sample. This clearly indicates the faster PL quenching is obtained in sample with Ti^{4+}-0.1% (Fig.4c). These TR-PL results also point out the 0.1% Ti^{4+} dopant in perovskite is convenient for charge transport and weakening the recombination of carriers (Table 2).

2.4 Performance of the solar cell devices

The performances with different Ti^{4+} contents in perovskite were measured to seek for optimum Ti^{4+} concentration, and the detailed photovoltaic parameters were displayed in Table 3 and Fig.5(a,b). Fig. 5c is the *J-V* curves of different Ti^{4+} contents doped devices. The pure PSCs shows J_{SC}=21.4 mA·cm^{-2}, V_{OC}= 1.09 V, FF=0.611, and E_{ff}=14.0% (E_{ff} is the efficiency). Ti^{4+}-0.1% acquires maximum J_{SC} of 22.3 mA·cm^{-2}. The FF gradually improves when the content in perovskite of Ti^{4+} increase, and FF achieves the highest value of 72.4% with Ti^{4+}-0.1%. Then, FF reduces once Ti^{4+} is over 0.1%. Finally, the best perfor-mance is 17.4% with Ti^{4+}-0.1% in PSCs. The effici-ency distribution is provided in supporting information (Fig. S1) and the average values are approximate 14.0% and 17.4%.

To investigate the recombination process of the devices with grain boundary passivation, the Nyquist

Table 3 Photovoltaic parameters of planar PSCs with different Ti^{4+} contents

Sample	J_{sc} / (mA·cm^{-2})	V_{oc} / V	FF / %	E_{ff} / %
Ti^{4+}-0%	21.4	1.09	61.1	14.0 (13.3±1.1)
Ti^{4+}-0.05%	21.2	1.10	65.2	15.2 (14.3±0.84)
Ti^{4+}-0.1%	22.3	1.10	72.4	17.4 (16.5±0.90)
Ti^{4+}-0.2%	20.1	1.10	63.7	14.1 (13.8±0.74)
Ti^{4+}-0.5%	19.8	1.08	54.0	11.7 (11.3±0.63)

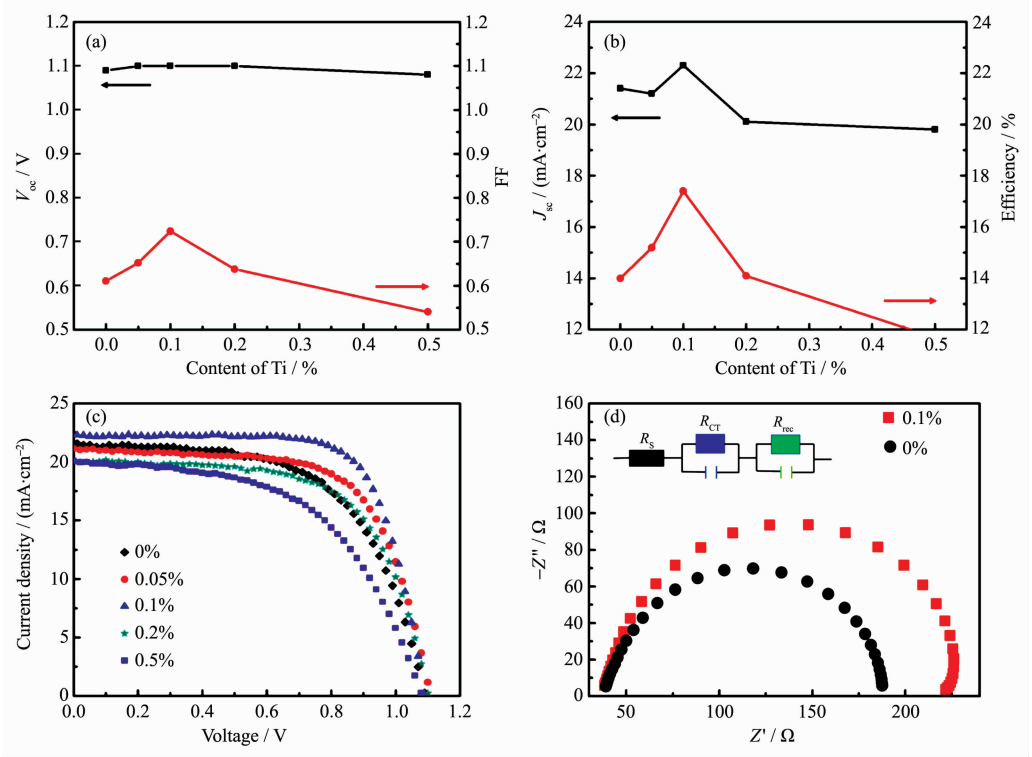

Fig.5 Variation of V_{OC}, FF (a) and J_{sc}, E_{ff} (b) with Ti^{4+} content; (c) *J-V* characteristics of device with different degree of Ti^{4+} in the perovskite layer; (d) Nyquist pot of the device with and without Ti^{4+} (measured at −1.1 V in the dark)

plots were obtained. In Fig.5d, the Nyquist plots of the devices were measured in the dark with bias voltage of −1.1 V. There are two semicircles in each Nyquist plot: the left one is related to the charge transport resistance (R_{ct}), which is mainly ascribed to charge extraction and separation at the interface between HTL or ETL and the perovskite layer. The right one is related to the photo carrier recombination resistance (R_{rec}) in the PSCs system; the starting point′s real part represents the series resistance (R_s) of the solar cells. The relevant equivalent circuit is shown in the insert in Fig.5b[30-31]. At applied reverse bias, it demonstrates the devices with Ti^{4+}-0.1% has larger recombination resistance of 220 Ω, much higher than 180 Ω of the undoped device, which indicates the recombination is effectively reduced by Ti^{4+} modification. Furthermore, the R_s is reduced to 18 Ω with Ti^{4+} doped device compared with 29 Ω of the undoped one. It is ascribed to the better crystallinity and more compactness of Ti^{4+} doped perovskite films reduce the contact resistance of the device.

The variation of photovoltaic parameters coincides with the analysis about device (Fig.5(c,d)). It is easy to know J_{SC} depends on the density of trap states, because they have a great compact on carrier recombination. With Ti^{4+}-0.1% doped in perovskite, the grain boundary trap states are effectively removed by Ti^{4+} and the device shows large recombination resistance and series resistance is effectively reduced. These merits increasing the rate of carrier transport from perovskite layer to electrodes. FF is also correlated with the density of trap states and interface contact[32]. Because of the fewer trap states, carriers are more apt to transfer to electrodes, which means the device has good FF (FF of Ti^{4+}-0.1% has effectively improved from 61.1% to 72.4%). Duo to these parameters being enhanced, efficiency of devices exhibits better performances with Ti^{4+}-0.1%. Experiments proof small dopants about Ti^{4+} ions will contribute to higher photovoltaic parameters as a result of defect passivation. But devices with more dopants (Ti^{4+} with 0.2%~0.5%) exhibit awful performance on account of more defects, which has bad effect on performances of devices.

3 Conclusions

In this work, photovoltaic properties get improved with small dopant content of Ti^{4+} in $MAPbI_3$ perovskite films. At the same time, the XRD analysis and SEM-mapping indicates the Ti^{4+} is most likely to accumulate at the grain boundary. The steady PL and TR-PL importantly support more powerful ability about carrier transport after Ti^{4+} doping. The Nyquist plots indicate the Ti^{4+} doping effectively reduce the interface recombination and improve the charge transport in the device. Therefore, the grain boundary defect states is effectively reduced by Ti^{4+} modification. Therefore, the device with optimal Ti^{4+} content shows excellent J_{SC}, V_{OC} and FF. Ti-0.1% shows the highest efficiency (17.4%) with doped device under 1sun (AM1.5).

Acknowledgments: This work was supported by the National Natural Science Foundation of China (Grant No.11374168, 11547033), Natural Science Foundation of Zhejiang Province (Grant No.LY18F040004), Scientific Research Foundation for the Returned Overseas Chinese Scholars and the K.C. Wong Magna Fund in Ningbo University, China.

Supporting information is available at http://www.wjhxxb.cn

References:

[1] Kojima A, Teshima K, Shirai Y, et al. *J. Am. Chem. Soc.*, **2009**,**131**(17):6050-6051

[2] Liu M, Johnston M, Snaith H. *Nature*, **2013**,**501**(7467):395-398

[3] Yang W, Park B, Jung E, et al. *Science*, **2017**,**356**(6345):1376-1379

[4] https://www.nrel.gov/pv/assets/images/efficiency-chart.png.

[5] LU Xing-Rong(陆新荣), ZHAO Yin(赵颖), LIU Jian(刘建), et al. *Chinese J. Inorg. Chem.*(无机化学学报), **2015**,**31**(9):1678-1686

[6] Tress W, Marinova N, Ingans O, et al. *Adv. Energy Mater.*, **2015**,**5**(3):1423-1427

[7] Zhou H P, Chen Q, Li G, et al. *Science*, **2014**,**6**:346-349

[8] Kim J, Lee S H, Lee J H. *J. Phys. Chem. Lett.*, **2014**,**5**(8):1312-1317

[9] Niu T Q, Lu J, Munir R, et al. *Adv. Mater.*, **2018**,**30**:1706576

[10]Wu X, Trinh M T, Niesner D, et al. *J. Am. Chem. Soc.*, **2015**,**137**(5):2089-2096

[11]Son D Y, Kim S G, Seo J Y, et al. *J. Am. Chem. Soc.*, **2018**, **140**(4):1358-1364

[12]Fang X, Ding J N, Yuan N Y, et al. *Phys. Chem. Chem. Phys.*, **2017**,**19**(8):6057-6063

[13]Huang X, Guo H, Wang K, et al. *Org. Electron.*, **2017**,**41**: 42-48

[14]Zhang J, Hu Z L, Huang L K, et al. *Chem. Commun.*, **2015**, **51**(32):7047-7050

[15]Qin P L, Yang G, Ren Z W, et al. *Adv. Mater.*, **2018**,**30**(12): 1706126

[16]Zhao W, Yao Z G, Yu F Y, et al. *Adv. Sci.*, **2018**,**5**(2):1700131

[17]Abdi-Jalebi M, Andaji-Garmaroudi Z, Cacovich S, et al. *Nature*, **2018**,**555**:497-501

[18]Chen R J, Hou D G, Lu C J, et al. *Sustainable Energy Fuels*, **2018**,**2**(5):1093-1100

[19]Zhang J, Shang M H, Wang P, et al. *ACS Energy Lett.*, **2016**,**1**(3):535-541

[20]Burschka J, Pellet N, Moon S J, et al. *Nature*, **2013**,**499** (7458):316-319

[21]Lee M M, Teuscher J, Miyasaka T, et al. *Science*, **2012**,**338** (6107):643-647

[22]Zhou Z M, Pang S P, Liu Z H, et al. *J. Mater. Chem.*, **2015**, **3**(38):19205-19217

[23]Abdi-Jalebi M, Andaji-Garmaroudi Z, Cacovich S. *Nature*, **2018**,**555**(7697):497-501

[24]Bush K A, Palmstrom A F, Yu Z J, et al. *Nat. Energy*, **2017**, **2**(4):17009

[25]Eperon G E, Leijtens T, Bush K A, et al. *Science*, **2016**,**354** (6314):861-865

[26]Mcmeekin D P, Sadoughi G, Rehman W, et al. *Science*, **2016**,**351**(6269):151-155

[27]Yamada Y, Nakamura T, Endo M, et al. *J. Am. Chem. Soc.*, **2014**,**136**(33):11610-11613

[28]Liu J, Shirai Y, Yang X D, et al. *Adv. Mater.*, **2015**,**27**(33): 4918-4923

[29]Chang J J, Lin Z H, Zhu H. *J. Mater. Chem. A*, **2016**,**4**(42): 16546-16552

[30]Pockett A, Eperon G E, Peltola T, et al. *J. Phys. Chem. C*, **2015**,**119**(7):3456-3465

[31]Dualeh A, Moehl T, Tetreault N. *ACS Nano*, **2014**,**8**(1):362-373

[32]Zhang J, Chen R J, Wu Y Z, et al. *Adv. Energy Mater.*, **2018**,**8**(5):1701981